Catalysis Science & Technology

PAPER

View Article Online
View Journal | View Issue

Cite this: *Catal. Sci. Technol.*, 2014, 4, 3705

Hydrodeoxygenation of fatty acids and triglycerides by Pt-loaded Nb_2O_5 catalysts

Kenichi Kon,[a] Wataru Onodera,[a] Satoru Takakusagi[a] and Ken-ichi Shimizu*[ab]

Received 10th June 2014,
Accepted 26th June 2014

DOI: 10.1039/c4cy00757c

www.rsc.org/catalysis

Platinum nanoparticles loaded onto various supports have been studied for the selective hydrogenation of lauric acid to *n*-dodecane. The activity depends on the support material and pre-reduction temperature. Pt/Nb_2O_5 reduced at 300 °C gives the highest activity. Pt/Nb_2O_5 shows higher activity than various Nb_2O_5-supported transition metals (Ir, Re, Ru, Pd, Cu, Ni). Under solvent-free conditions Pt/Nb_2O_5 is effective for the hydrodeoxygenation of lauric, capric, palmitic, myristic, oleic, and stearic acids under 8 bar H_2 at 180–250 °C, which gives high yields (88–100%) of linear alkanes with the same chain length as the starting compound. Tristearin is also converted to give 93% yield of *n*-octadecane. Pt/Nb_2O_5 shows more than 60 times higher turnover number (TON) than the previously reported catalysts for the hydrogenation of stearic acid to *n*-octadecane. Mechanistic study shows a consecutive reaction pathway in which lauric acid is hydrogenated to 1-dodecanol, which undergoes esterification with lauric acid as well as hydrogenation to *n*-dodecane. The ester undergoes hydrogenolysis to give the alcohol, which is hydrogenated to the alkane. Infrared (IR) study of acetic acid adsorption on Nb_2O_5 indicates that Lewis acid–base interaction of Nb cation and carbonyl oxygen, which suggests a possible role of Nb_2O_5 as an activation site of carbonyl groups during hydrodeoxygenation.

Introduction

Developing alternative fuels from non-food biomass has become a key factor to ensure sustainable growth by minimizing the carbon footprint. In this context, triglycerides and fatty acids have been identified as promising resources of biodiesel,[1–5] because they can be easily and economically produced from microalgae which have rapid growth rate and high lipid content. As comprehensively reviewed by Murzin *et al.*,[2] three upgrading processes, cracking, transesterification and deoxygenation, have been developed to produce biodiesel. Deoxygenation of triglyceride/fatty acid feed under hydrogen is of particular importance, because the reaction reduces the high-oxygen content and related acidity of fatty acids, yielding saturated hydrocarbons suitable for drop-in diesel fuel. As comprehensively described by Lercher *et al.*[1] and Bitter *et al.*,[3] the catalytic deoxygenation of biomass-derived fatty acid derivatives can be classified into three reactions: decarbonylation, decarboxylation and hydrodeoxygenation. Decarbonylation and decarboxylation yield hydrocarbons with one carbon atom less than the fatty acids, while hydrodeoxygenation gives hydrocarbons with the same chain length as the starting compound. Hydrodesulfurization catalysts (sulfided CoMo or NiMo oxides), which are selective to hydrodeoxygenation,[6,7] can suffer from sulfur leaching. In contrast, most of the supported group 9 and 10 metal catalysts,[8–15] such as Ni/ZrO_2 (ref. 8) and supported Pd, Pt, and Rh catalysts,[9–13] are highly selective to decarbonylation or decarboxylation products even in the presence of H_2. A few catalysts (Ni-loaded zeolites,[16] Pt-Re/ZSM-5,[17] and tungsten and molybdenum carbides[18–21]) have been reported to be effective for the selective transformation of fatty acids into diesel-range alkanes without a loss of the chain length of the corresponding fatty acid at 260–350 °C under 10–50 bar H_2. However, they still have problems such as high catalyst loading (low turnover number (TON)), formation of small amounts of decarbonylation and cracking by-products and the need for high pressure H_2 and high temperature. In this paper we report on the selective and quantitative hydrodeoxygenation of stearic acid to *n*-octadecane under milder conditions (180 °C, 2 or 8 bar H_2) than that in the previous studies using Pt/Nb_2O_5, which shows more than two orders of magnitude higher TON than Pt/SiO_2 and previous catalysts for the selective hydrodeoxygenation of fatty acids. Substrate scope, kinetic and *in situ* IR studies are also carried out to discuss the catalytic performance, reaction pathways, and a possible role of Nb_2O_5 in the present catalytic system.

[a] *Catalysis Research Center, Hokkaido University, N-21, W-10, Sapporo 001-0021, Japan. E-mail: kshimizu@cat.hokudai.ac.jp; Fax: +81 11 706 9163*
[b] *Elements Strategy Initiative for Catalysts and Batteries, Kyoto University, Katsura, Kyoto 615-8520, Japan*

Experimental

General

Commercially available organic compounds (from Tokyo Chemical Industry or Kanto Chemical) were used without further purification. GC (Shimadzu GC-14B) and GC-MS (Shimadzu GCMS-QP2010) analyses were carried out with an Ultra ALLOY capillary column UA$^+$-1 (Frontier Laboratories Ltd.) using nitrogen and He as carrier gases.

Catalyst preparation

Nb_2O_5 (54 m^2 g^{-1}) was prepared by the calcination of niobic acid ($Nb_2O_5{\cdot}nH_2O$, kindly supplied by CBMMI) at 500 °C for 3 h. SiO_2 (Q-10, 300 m^2 g^{-1}) was supplied by Fuji Silysia Chemical Ltd. H^+-type MFI zeolite (HMFI) with a SiO_2/Al_2O_3 ratio of 22.3 was kindly supplied by Tosoh Co. HBEA zeolite (JRC-Z-HB25, SiO_2/Al_2O_3 = 25 ± 5), silica-alumina (JRC-SAL-2, SiO_2/Al_2O_3 = 5.6), MgO (JRC-MGO-3), TiO_2 (JRC-TIO-4), CeO_2 (JRC-CEO-3) was supplied by the Catalysis Society of Japan. γ-Al_2O_3 was prepared by the calcination of γ-AlOOH (Catapal B Alumina purchased from Sasol) for 3 h at 900 °C. ZrO_2 was prepared by the calcination (500 °C for 3 h) of $ZrO_2{\cdot}nH_2O$ prepared by the hydrolysis of zirconium oxynitrate 2-hydrate in water by aqueous NH_4OH solution followed by filtration of the precipitate, washing with water three times, and drying at 100 °C.

The precursor of Pt/Nb_2O_5 was prepared by an impregnation method. A mixture of Nb_2O_5 and an aqueous HNO_3 solution of $Pt(NH_3)_2(NO_3)_2$ was evaporated at 50 °C followed by drying at 90 °C for 12 h. Before each catalytic experiment, the Pt/Nb_2O_5 catalyst (with a Pt loading of 5 wt%) was prepared by *in situ* pre-reduction of the precursor in a Pyrex tube under a flow of H_2 (20 cm^3 min^{-1}) at 300 °C for 0.5 h. Other supported Pt catalysts (Pt = 5 wt%) were prepared by the same method. Nb_2O_5-supported metal catalysts, M/Nb_2O_5 (M = Ni, Cu, Ru, Pd, Ag, Re, Ir) with a metal loading of 5 wt%, were prepared by the impregnation method similarly to Pt/Nb_2O_5 using an aqueous solution of metal nitrates (for Co, Ni, Cu, Ag), $RuCl_3$, $IrCl_3{\cdot}nH_2O$, NH_4ReO_4 or an aqueous HNO_3 solution of $Pd(NO_3)_2$. A commercial Pt-loaded carbon catalyst (Pt/C, Pt = 5 wt%) was purchased from N.E. Chemcat Corporation.

Characterization

Temperature-programmed reduction under H_2 (H_2-TPR) was carried out using a BELCAT (BELL Japan Inc.). The unreduced precursor of Pt/Nb_2O_5, $Pt(NH_3)_2(NO_3)_2$-loaded Nb_2O_5 (20 mg), was mounted in a quartz tube, and the sample was heated with a ramp rate of 2 °C min^{-1} in a flow of 5% H_2/Ar (20 cm^3 min^{-1}). The effluent gas was passed through a trap containing MS 4 Å to remove water, and then through the thermal conductivity detector. The amount of H_2 consumed during the experiment was detected by a thermal conductivity detector.

The number of surface metal atoms in Pt/Nb_2O_5, pre-reduced in H_2 at 300 °C for 0.5 h, was estimated from the CO uptake of the samples at room temperature using the pulse-adsorption of CO in a flow of He using a BELCAT. The average particle size was calculated from CO uptake assuming that CO was adsorbed on the surface of spherical Pt particles at 1:1 CO/(surface Pt atom) stoichiometry.

TEM measurements were carried out by using a JEOL JEM-2100F TEM operated at 200 kV.

In situ IR spectra were recorded using a JASCO FT/IR-4200 equipped with an MCT detector. For the IR studies of CO and pyridine adsorption, we used a flow-type IR cell connected to a flow reaction system. For the IR study of acetic acid adsorption, we used a closed IR cell connected to an evacuation system. The sample was pressed into a 40 mg self-supporting wafer (ϕ = 2 cm) and mounted into the IR cell with CaF_2 windows. Spectra were measured by 15 accumulated scans at a resolution of 4 cm^{-1}. A reference spectrum of the catalyst wafer in He taken at the measurement temperature was subtracted from each spectrum. For the CO-IR study, a disk of Pt/Nb_2O_5 was heated in H_2 flow (20 cm^3 min^{-1}) at 300 °C for 0.5 h followed by exposure to a flow of CO(5%)/He (20 cm^3 min^{-1}) for 180 s at 40 °C and by purging with He for 600 s. Then, IR measurement was carried out. For the pyridine-IR study, the Pt/Nb_2O_5 disc, pre-reduced in H_2 at 300 °C for 0.5 h, was exposed to 1 μL of liquid pyridine vaporized at 200 °C under He flow at 150 °C. Then, the disk was purged with He for 600 s, and IR measurement was carried out. During the acetic acid-IR study, the IR cell was cooled in an ice bath, and the thermocouple near the sample showed 8 ± 1 °C. The sample disc (Nb_2O_5 or SiO_2) in the closed IR cell, pre-evacuated at 500 °C for 0.5 h, was exposed to 20 Pa of acetic acid at 8 °C for 600 s, and then IR spectra were measured at 8 °C.

Typical procedures of catalytic reactions

Pt/Nb_2O_5 (0.07, 0.2 or 1 mol% Pt with respect to carboxylic acid) pre-reduced at 300 °C was used as the standard catalyst. The other catalysts were also pre-reduced at 300 °C before reaction. After pre-reduction, the catalyst in the closed glass tube sealed with a septum inlet was cooled to room temperature under H_2. A mixture of carboxylic acid (1 mmol) and *n*-decane or *n*-dodecane (0.2 mmol) was injected to the pre-reduced catalyst inside the glass tube through the septum inlet. Then, the septum was removed under air, and a magnetic stirrer was put in the tube, followed by the insertion of the tube inside a stainless autoclave with a dead space of 28 cm^3. After sealing, the reactor was flushed with H_2 from a high pressure gas cylinder and charged with H_2 (typically 8 bar) at room temperature. Then, the reactor was heated typically at 180 °C under stirring (150 rpm). After the reaction, acetone (10 cm^3) was added to the mixture, and the conversion and yields of products were determined by GC using *n*-decane or *n*-dodecane as an internal standard. The products were identified by GC-MS equipped with the same column as in GC and by comparison with commercially available products.

Results and discussion

Characterization of Pt/Nb_2O_5

We characterized the structure of the representative catalyst Pt/Nb_2O_5 pre-reduced at 300 °C. The H_2-TPR of the unreduced precursor, $Pt(NH_3)_2(NO_3)_2$-loaded Nb_2O_5, is shown in Fig. 1. H_2 consumption due to the reduction of oxidic Pt to metallic Pt is observed mostly below 100 °C. Fig. 2 shows the particle size distribution of Pt/Nb_2O_5 obtained from transmission electron microscopy (TEM) analysis. The volume-area mean diameter of the Pt particle was 4.7 nm. The number of exposed Pt^0 sites estimated by the CO adsorption amount (28.3 μmol g^{-1}-cat) is smaller than the number of surface Pt atoms (39.4 μmol g^{-1}-cat) estimated by using the volume-area mean diameter of Pt from TEM and by assuming that CO is adsorbed on the surface of spherical Pt particles at a CO/(surface Pt atom) stoichiometry of 1:1. This result is consistent with the previous result that an increase in the H_2-treatment temperature of Pt/Nb_2O_5 leads to a decrease in hydrogen and CO uptake on the catalyst.[22–24] This phenomenon has been generally called the strong metal–support interaction (SMSI),[22–34] where a metal surface is partially covered with suboxide (NbO_x) species produced by the partial reduction of the support (Nb_2O_5) at high temperatures (200–500 °C). The SMSI phenomenon was also observed in Nb_2O_5-supported Pd, Rh and Ir catalysts.[26–28] The IR study of CO adsorption on Pd/Nb_2O_5 showed that an increase in the reduction temperature of Pd/Nb_2O_5 from 100 °C to 300 °C resulted in the suppression of the band at 1938 cm^{-1} due to the bridged CO on Pd.[27] This observation was assigned to the blocking of the Pd surface by migrated NbO_x species. As shown in Fig. 3, our IR data for CO adsorption on Pt/Nb_2O_5 gave similar results. The IR spectrum of CO on Pt/Nb_2O_5 reduced at 100 °C showed bands in the 2000–2080 cm^{-1} range due to linearly coordinated CO on Pt^0 and at 1840 cm^{-1} due to bridged CO on the flat surface of Pt.[24] The increase in the reduction temperature of Pt/Nb_2O_5 from 100 °C to 300 °C resulted in the large suppression of the bridged CO band and the linear CO bands (especially at low wavenumber regions). The result supports the SMSI model of Pt/Nb_2O_5 reduced at 300 °C, where the Pt surface is partly covered with NbO_x species. Summarizing the structural results, it is concluded that the dominant Pt species in Pt/Nb_2O_5 pre-reduced at 300 °C are Pt metal particles whose surface is partially covered with NbO_x species.

Optimization of catalysts and conditions

We studied the influence of various catalyst parameters on the catalytic activity for the hydrogenation of lauric acid under solvent-free conditions and 8 bar H_2 at 180 °C for 4 h using 1 mol% catalyst (Table 1). First, various metal (M)-loaded Nb_2O_5 catalysts (M = Pt, Ir, Ru, Re, Pd, Cu, Ni), pre-reduced at 300 °C, were studied (entries 2–8). It was found that Pt/Nb_2O_5 showed the highest yield of *n*-dodecane. 1-Dodecanol and

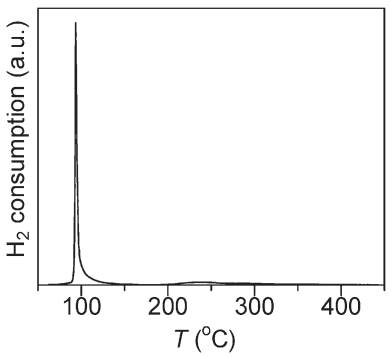

Fig. 1 H_2-TPR profile of the unreduced precursor of Pt/Nb_2O_5.

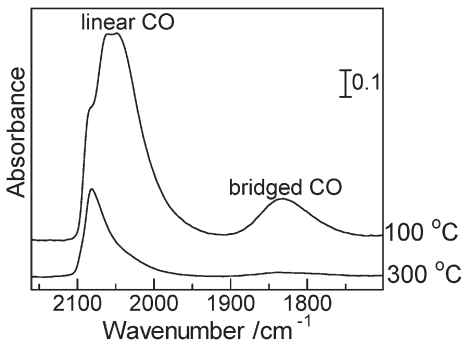

Fig. 3 IR spectra (40 °C) of CO adsorbed on Pt/Nb_2O_5 pre-reduced at 100 and 300 °C.

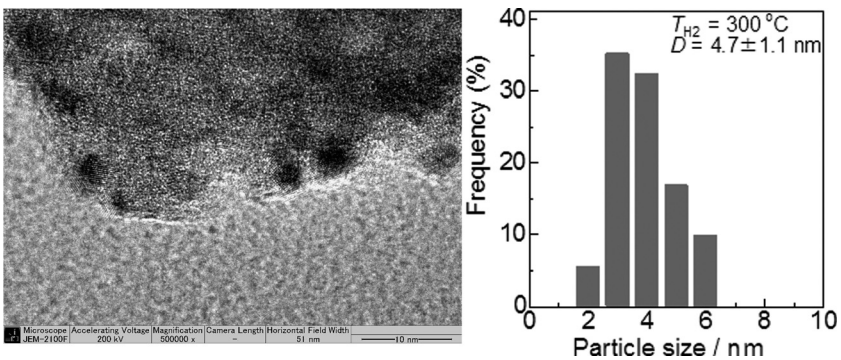

Fig. 2 Representative TEM image and Pt particle size distribution of Pt/Nb_2O_5 (pre-reduced at 300 °C). The volume-area mean diameter of the Pt particle was 4.7 ± 1.1 nm.

Table 1 Hydrogenation of lauric acid by 5 wt% metal-loaded catalysts

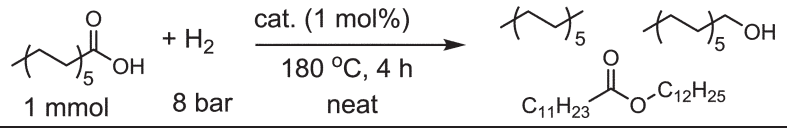

Entry	Catalyst	Conv. (%)	Yield (%)		
			Dodecane	Dodecanol	Ester[a]
1	Nb_2O_5	29	0	0	0
2	Pt/Nb_2O_5	100	60	7	21
3	Ir/Nb_2O_5	86	19	12	31
4	Ru/Nb_2O_5	73	4 (8)[c]	9	29
5	Re/Nb_2O_5	23	1	0	4
6	Pd/Nb_2O_5	21	1	0	4
7	Cu/Nb_2O_5	24	1	0	0
8	Ni/Nb_2O_5	23	0.4	0	0
9	Pt/Nb_2O_5[b]	93	16	11	36
10	Pt/niobic acid	98	13	19	24
11	Pt/C	2	1	0	0
12	Pt/SiO_2	1	0	0	0
13	Pt/TiO_2	82	6	13	41
14	Pt/SiO_2–Al_2O_3	42	3	0	1
15	Pt/BEA	8	2	0	2
16	Pt/MFI	61	1	0	1
17	Pt/ZrO_2	14	2	0	9
18	Pt/Al_2O_3	14	1	0	1
19	Pt/CeO_2	2	1	0	2
20	Pt/MgO	44	1	3	0

[a] Dodecyl dodecanoate. [b] Pre-reduced at 100 °C for 0.5 h. [c] Undecane.

dodecyl dodecanoate were also produced as by-products. Next, we screened a series of supported Pt catalysts pre-reduced at 300 °C (entries 2, 10–20). The activity depended strongly on the support materials, and Pt/Nb_2O_5 (entry 2) showed more than 10 times higher yield of *n*-dodecane (60%) than the other Pt-loaded metal oxides (entries 10–20). Pt/TiO_2 (entry 13) and niobic acid-supported Pt (entry 10) also showed high conversions, but these catalysts gave partially reduced products (dodecyl dodecanoate and 1-dodecanol) as main products. Pt metal particles on an inert support (Pt/SiO_2, entry 12) and Nb_2O_5 itself (entry 1) showed no yield of dodecane, indicating that the Pt metal particles and the support itself could not catalyze the reaction under the present conditions. The Pt/Nb_2O_5 catalyst reduced at 100 °C (entry 9) showed a lower yield of *n*-dodecane (16%) than that reduced at 300 °C (60%).

With the most effective catalyst, Pt/Nb_2O_5 reduced at 300 °C, we studied the optimization of reaction conditions. Fig. 4 shows the effect of hydrogen pressure on conversion and product yields for the reaction after 4 h. Note that the conversion and yield at a H_2 pressure of 0 bar correspond to the reaction under 1 bar N_2. The dodecane yield was highest at a H_2 pressure of 8 bar. Further increase in the H_2 pressure decreased the yield of dodecane and increased those of dodecanol and ester. This may suggest a competitive activation of hydrogen and lauric acid at the same catalytic site under high H_2 pressure.

Fig. 5 shows the time course of the reaction under solvent-free conditions at 180 °C and 8 bar H_2. Note that the conversion and yield at t = 0 h were measured after addition of the reaction mixture to the pre-reduced Pt/Nb_2O_5 under ambient conditions. The profile is characteristic of the consecutive reaction mechanism; 1-dodecanol and dodecyl dodecanoate, formed at an initial induction period, were consumed after 1 h to give the over-hydrogenated product *n*-dodecane. After 24 h, the yield of *n*-dodecane was 99%, and no formation of by-products was observed from GC-MS analysis. Next, we tested the reaction under 8 bar H_2 for 24 h in different solvents (Table 2). The reaction under solvent-free conditions gave the highest yield (99%) of *n*-dodecane. The reaction in toluene also gave a good yield (90%). The use of

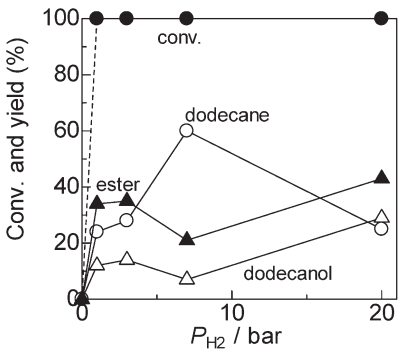

Fig. 4 Effect of H_2 pressure on the conversion and product yields of lauric acid hydrogenation by Pt/Nb_2O_5 (pre-reduced at 300 °C).

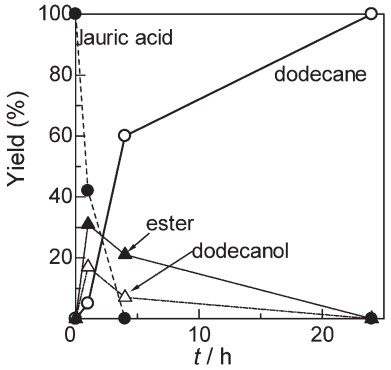

Fig. 5 Time-conversion profile of lauric acid hydrogenation by Pt/Nb_2O_5 (pre-reduced at 300 °C).

Table 2 Hydrogenation of lauric acid by Pt/Nb_2O_5[a]

Solvent	Conv. (%)	Yield (%)		
		n-Dodecane	1-Dodecanol	Ester[b]
Solvent-free	100	99	0	0
Toluene	100	90	9	2
o-Xylene	100	42	12	39
Mesitylene	100	31	17	45
Diglyme	100	43	17	40
H_2O	97	40	49	10

[a] Conditions: lauric acid (1 mmol), catalyst (1 mol%), solvent (0.3 g), 180 °C, 8 bar H_2, 24 h. [b] Dodecyl dodecanoate.

o-xylene, mesitylene, diglyme and water resulted in moderate yields (31–43%) with 1-dodecanol and dodecyl dodecanoate as by-products.

Performance of Pt/Nb_2O_5-catalyzed hydrogenation of fatty acids

From the above optimization experiments, we found the best conditions (8 bar H_2, 24 h, 180 °C, 1 mol% Pt/Nb_2O_5, without solvent), which gave a quantitative dodecane yield without any by-products (Table 3, entry 1). ICP-AES analysis of the solution after the reaction confirmed that the contents of Pt and Nb in the solution were below the detection limits. After the standard reaction for 24 h, the catalyst was separated from the reaction mixture by centrifugation and was dried at 90 °C for 12 h and then reduced in H_2 at 300 °C for 0.5 h. The recovered catalyst showed quantitative yields of *n*-dodecane (Table 3, entries 2, 3). These results indicate that Pt/Nb_2O_5 acts as a reusable heterogeneous catalyst for this reaction. It is important to note that this system is effective even under a low H_2 pressure of 2 bar, giving a quantitative yield (eqn (1)).

As summarized in Table 3, the scope of liquid-phase hydrogenation using Pt/Nb_2O_5 under solvent-free conditions was further expanded to various fatty acids and tristearin. The reactions of capric, palmitic, myristic, oleic, and stearic acids under low hydrogen pressure (8 bar) at 180–250 °C resulted in high yields (88–99%) of linear alkanes with the same chain length as the starting compound, and the yields of by-products (lower or branched alkanes, alcohols and esters) were below the detection limit of GC analyses. Tristearin was also converted to give an *n*-octadecane yield of 93%. Another important aspect of this catalytic system is a high TON. As shown in entry 8, the hydrogenation of 2 mmol of stearic acid in the presence of a small amount of the catalyst (0.07 mol%) at 250 °C under 8 bar H_2 resulted in an *n*-octadecane yield of 96%, corresponding to a TON of 1371 with respect to the total number of Pt atoms in the catalyst. As compared in Table 4, this value is more than 60 times higher than those of previously reported heterogeneous catalysts. Under the same conditions, Pt/SiO_2 gave no yield of *n*-octadecane but gave 7% yield of a hydrocarbon with one carbon atom less than the fatty acids.

Reaction pathways

The kinetic profile for the hydrogenation of lauric acid (Fig. 5) indicates the consecutive reaction pathway; dodecanol and dodecyl dodecanoate, formed at an initial induction period, are hydrogenated to yield dodecane as the final product. To give further evidence of the tentative mechanism, we compared the initial rates of the individual steps. Table 5 lists the initial formation rates of the products for the hydrogenation of lauric acid, 1-dodecanal, 1-dodecanol or dodecyl dodecanoate (ester), together with the ester formation rate by the reaction of lauric acid with 1-dedecanol. For the hydrogenation of lauric acid, the formation of *n*-dodecane (5 mmol h^{-1}) is slower than the formation of 1-dodecanol (17 mmol h^{-1}) and the ester (31 mmol h^{-1}). The hydrogenation of 1-dodecanal, 1-dodecanol and dodecyl dodecanoate resulted in the formation of *n*-dodecane as the main product. The order of the *n*-dodecane formation rate is as follows: dodecanal (15 mmol h^{-1}) > dodecanol (13 mmol h^{-1}) > dodecyl dodecanoate (8 mmol h^{-1}) > lauric acid (5 mmol h^{-1}). Considering the fact that the esterification of lauric acid with 1-dodecanol (63 mmol h^{-1}) shows the highest rate in the reactions in Table 5, we propose a possible reaction pathway in Scheme 1. The carboxylic acid is hydrogenated to an alcohol possibly *via* an aldehyde. However, the fact that 1-dodecanol is not produced by the hydrogenation of 1-dodecanal (entry 2 in Table 5) suggests a direct hydrogenation of carboxylic acid to alcohol. The alcohol

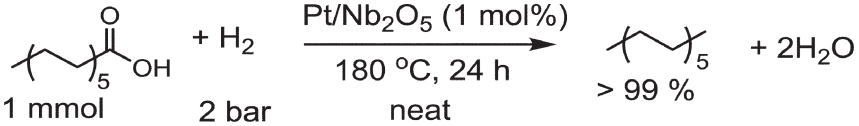

(1)

Table 3 Hydrogenation of fatty acids by Pt/Nb_2O_5[a]

Entry	Fatty acid	Pt (mol%)	T (°C)	t (h)	Conv. (%)	Yield (%)		
						n-C_nH_{2n+2}[b]	Alcohol	Ester
1	Lauric acid	1	180	24	100	99	0	0
2[c]		1	180	24	100	99	0	0
3[d]		1	180	24	100	99	0	0
4	Capric acid	1	180	24	100	88	0	0
5	Palmitic acid	0.2	250	24	100	90	0	0
6	Myristic acid	0.2	250	24	100	89	0	0
7	Oleic acid	0.2	250	24	100	99	0	0
8[e]	Stearic acid	0.07	250	48	100	96	0	0
9[f]	Tristearin	1	260	24	100	93	0	0

[a] 1 mmol of fatty acid, solvent-free, 8 bar H_2. [b] Linear alkanes with the same chain length as the starting compound. [c] 1st reuse. [d] 2nd reuse. [e] 2 mmol of stearic acid, 8 bar H_2. [f] 1 mmol of tristearin, 50 bar H_2, 1 mol% Pt cat. with respect to the carboxyl group.

Table 4 Heterogeneous catalysts for the hydrogenation of stearic acid to octadecane[a]

Catalyst	mol%	T (°C)	t (h)	P_{H_2} (bar)	Yield (%)	TOF (h^{-1})	TON	Ref.
Pt/Nb_2O_5	0.07	250	48	8	96	29	1371	This study[a]
Pt/SiO_2	0.07	250	48	8	0 (7)[b]	—	—	This study[a]
Ni/HBEA	9.65	260	8	40	97.3	1.3	10	16
Mo_2C/C	22.3	280	4	10	75	3.4	0.8	21
W-based cat.	2.9	350	5	50	67	4.6	23	18

[a] Conditions: 2 mmol of stearic acid, solvent-free, 8 bar H_2. [b] Yield of n-heptadecane.

Table 5 Hydrogenation of model compounds by Pt/Nb_2O_5[a]

Entry	Substrate	Initial rate/mmol h^{-1}		
		n-Dodecane	1-Dodecanol	Ester[b]
1	Lauric acid	5	17	31
2	1-Dodecanal	15	0	—
3	1-Dodecanol	13	—	—
4	Ester[b]	8	0	—
5[c]	Esterification	—	—	63

[a] Conditions: 1 mmol of the substrate, solvent-free, 1 mol% Pt catalyst, 180 °C, 8 bar H_2. [b] Dodecyl dodecanoate. [c] Esterification of lauric acid (1 mmol) with 1-dodecanol (1 mmol) at 180 °C in 1 atm N_2.

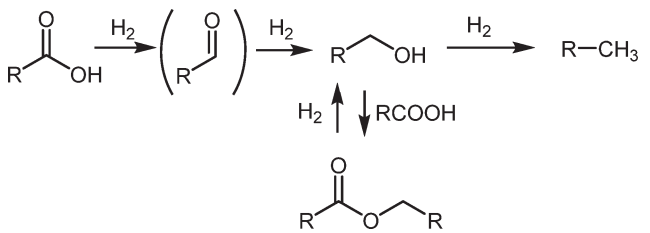

Scheme 1 Proposed reaction pathway for the hydrodeoxygenation of lauric acid by Pt/Nb_2O_5.

undergoes esterification with the carboxylic acid as well as hydrogenation to an alkane (dodecane). The ester undergoes hydrogenolysis to give the alcohol, which is hydrogenated to the alkane. During the model hydrogenation of dodecanol (Table 5, entry 2), we did not observe dodecene as a by-product, which excludes a possible formation of dodecane *via* the dehydration of the alcohol to alkene followed by its hydrogenation. The proposed pathway in Scheme 1 is consistent with that proposed by Lercher for the catalytic hydrogenation of stearic acid to octadecane over the Ni/HBA catalyst.[16] They proposed the production of octadecane by the consecutive pathway: stearic acid hydrogenation to 1-octadecanolΔ followed by 1-octadecanol hydrogenation to octadecane.

Possible role of Nb_2O_5

As discussed above, Pt/Nb_2O_5 showed a significantly higher activity than the other Pt-loaded catalysts and Nb_2O_5 itself, suggesting a synergy between Pt and Nb_2O_5 support. On the basis of our characterization results and the SMSI model of the Pt/Nb_2O_5 system in the literature,[22–24] we have concluded that the dominant Pt species in the most effective catalyst, Pt/Nb_2O_5 reduced at 300 °C, are the Pt metal particles whose surface is partly covered with NbO_x species. As shown in Table 1, the increase in the reduction temperature of Pt/Nb_2O_5 from 100 °C to 300 °C increased its activity for hydrodeoxygenation. The CO-IR results in Fig. 3 suggest that the increase in the reduction temperature of Pt/Nb_2O_5 from 100 °C to 300 °C resulted in a nearly complete blocking of the bridged site on a flat Pt surface by NbO_x species. Summarizing these results, the higher activity of the Pt/Nb_2O_5 catalyst reduced at 300 °C is explained by a partial decoration of Pt by NbO_x in which a relatively large number of Pt^0 atoms can be located at metal–NbO_x perimeter sites. Pt/TiO_2 is also a well known SMSI catalyst.[29–34] Table 1 shows that Pt/TiO_2 (reduced at 300 °C) is a moderately effective catalyst; it shows higher yields of dodecane and partially reduced products (dodecyl dodecanoate and dodecanol) than non-SMSI catalysts (such as Pt/C, Pt/SiO_2 and Pt/Al_2O_3). These results lead to a hypothesis that cooperation between Pt

metal and adjacent NbO_x (or TiO_x) species is responsible for high catalytic activity.

It is known that the partial blocking of Pt by suboxides (NbO_x or TiO_x) causes the formation of new perimeter sites between the Pt and the suboxide.[22–24] Yoshitake and Iwasawa[22] studied the hydrogenation of acrolein by the Pt/Nb_2O_5 catalyst in the SMSI state (reduced at 500 °C). They proposed that the higher selectivity in C=O bond reduction than C=C bond reduction is caused by cooperation between Pt and NbO_x at the perimeter sites, in which H_2 is dissociated by Pt and acrolein is activated by NbO_x. Vannice[29] also showed a significant enhancement in the selectivity in C=O bond reduction for the hydrogenation of crotonaldehyde by Pt/TiO_2 reduced at 500 °C. Somorjai and Bell showed that the activity of Rh foil for CO and CO_2 hydrogenation was increased by partially decorating the Rh surface with suboxides such as NbO_x, and the activity of the decorated Rh surface increased with an increase in the Lewis acidity of the suboxide.[37] This rate enhancement is attributed to the activation of the C=O bond *via* Lewis acid–base interactions between the cationic sites in the suboxide and the oxygen atom of CO or CO_2.[37–39] Enhanced selectivity or activity by metal–Lewis acid cooperation at the metal–oxide interface has been reported for various catalytic systems for the hydrogenation of C–O or C=O bonds.[22,26–31,35–43]

As evidenced by the IR band due to coordinated pyridine on the Lewis acid site (1445 cm^{-1}) in the pyridine adsorption IR experiment (Fig. 6), Pt/Nb_2O_5 has Lewis acid sites (exposed Nb^{n+} cations). Then, to evaluate the Lewis acid–base interactions between Nb cations and carbonyl oxygens of carboxylic acids in the present system, we carried out IR observations of acetic acid on Nb_2O_5. The spectrum in Fig. 7 shows the C=O stretching band of adsorbed acetic acid[30] at a lower wavenumber (1660 cm^{-1}) than that for the non-Lewis acidic oxide SiO_2 (1715 cm^{-1}). This indicates charge transfer from the oxygen atom of the carboxyl group (Lewis base) to the Nb^{5+} cation (Lewis acid) site of the Nb_2O_5 surface. Taking the discussion into consideration, we propose that the polarization of the C=O bond of the carboxylic acid by the Lewis acid–base interaction of Nb cation and carboxyl group is the primary important role of the Nb_2O_5 support in the present catalytic system (Scheme 2). The high activity of Pt/Nb_2O_5 can be caused by cooperation between Pt and NbO_x at the perimeter sites, in which H_2 is dissociated by Pt and carboxylic acid is activated by NbO_x *via* Lewis acid–base interactions. The increase in activity with an increase in the reduction temperature of Pt/Nb_2O_5 from 100 °C to 300 °C could be explained by an increase in the Pt–NbO_x perimeter length caused by the migration of NbO_x islands onto the Pt metal surface.

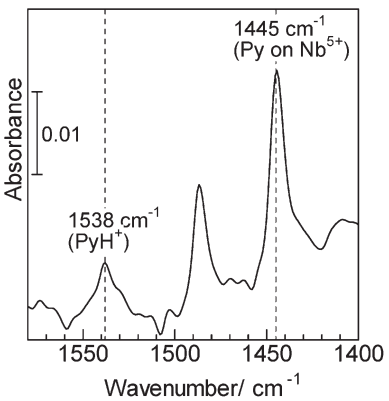

Fig. 6 IR spectra of pyridine adsorbed on Pt/Nb_2O_5 at 150 °C.

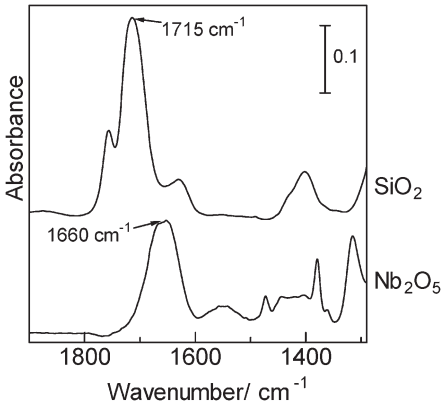

Fig. 7 IR spectra of acetic acid adsorbed on Nb_2O_5 and SiO_2 at 8 °C.

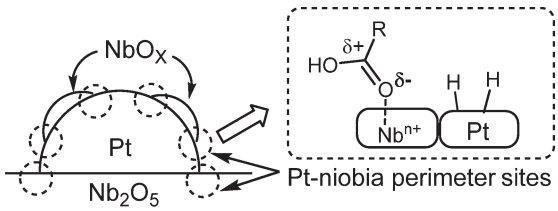

Scheme 2 Proposed cooperative mechanism of the hydrodeoxygenation of carboxylic acids by Pt/Nb_2O_5 in a partially SMSI state.

Conclusions

Pt/Nb_2O_5 is found to be an effective catalyst for the hydrodeoxygenation of lauric, capric, palmitic, myristic, oleic, and stearic acids at low H_2 pressure (8 bar) and 180–250 °C under solvent-free conditions, which give high yields of linear alkanes with the same chain length as the starting compound. Tristearin is also converted to give 93% yield of *n*-octadecane under 50 bar H_2 at 260 °C. Pt/Nb_2O_5 shows more than 60 times higher TON than previously reported catalysts for the hydrogenation of stearic acid to *n*-octadecane. Mechanistic study shows the following reaction pathways. Carboxylic acid is hydrogenated to alcohol, which undergoes esterification with a carboxylic acid as well as hydrogenation to alkane. The ester undergoes hydrogenolysis to give an alcohol, which is hydrogenated to an alkane. Pt/Nb_2O_5 in a partial SMSI state shows significantly higher activity than the non-SMSI catalysts. Combined with the IR evidence of the Lewis acid–base interaction between the surface Nb cation and the carboxyl oxygen of an adsorbed carboxylic acid, we propose that the high activity of Pt/Nb_2O_5 is caused by cooperation between Pt and NbO_x at the perimeter sites, in which H_2 is dissociated by Pt and carboxylic acid is activated by NbO_x *via* Lewis acid–base interactions.

Acknowledgements

This work was supported by a Grant-in-Aid for Scientific Research on Innovative Areas "Nano Informatics" (25106010) from JSPS and the MEXT program "Elements Strategy Initiative to Form Core Research Center".

Notes and references

1 C. Zhao, T. Brück and J. A. Lercher, *Green Chem.*, 2013, **15**, 1720–1739.
2 S. Lestari, P. Mäki-Arvela, J. Beltramini, G. Q. Max Lu and D. Yu. Murzin, *ChemSusChem*, 2009, **2**, 1109–1119.
3 R. W. Gosselink, S. A. Hollak, S.-W. Chang, J. van Haveren, K. P. de Jong, J. H. Bitter and D. S. van Es, *ChemSusChem*, 2013, **6**, 1576–1594.
4 F. Shi, P. Wang, Y. H. Duan, D. Link and B. Morreale, *RSC Adv.*, 2012, **2**, 9727–9747.
5 J. C. Serrano-Ruiz, E. V. Ramos-Fernandez and A. Sepulveda-Escribano, *Energy Environ. Sci.*, 2012, **5**, 5638–5652.
6 O. I. Senol, E. M. Ryymin, T. R. Viljava and A. O. I. Krause, *J. Mol. Catal. A: Chem.*, 2007, **268**, 1–8.
7 Y. Liu, R. Sotelo-Boyas, K. Murata, T. Minowa and K. Sakanishi, *Energy Fuels*, 2011, **25**, 4675–4685.
8 B. Peng, C. Zhao, S. Kasakov, S. Fortaita and J. A. Lercher, *Chem. – Eur. J.*, 2013, **19**, 4732–4741.
9 I. Kubičková, M. Snåre, K. Eränen, P. Mäki-Arvela and D. Yu. Murzin, *Catal. Today*, 2005, **106**, 197–200.
10 B. Rozmysłowicz, P. Mäki-Arvela, A. Tokarev, A.-R. Leino, K. Eränen and D. Y. Murzin, *Ind. Eng. Chem. Res.*, 2012, **51**, 8922–8927.
11 J. Han, H. Sun, Y. Ding, H. Lou and X. Zheng, *Green Chem.*, 2010, **12**, 463–467.
12 J. Han, H. Sun, J. Duan, Y. Ding, H. Lou and X. Zheng, *Adv. Synth. Catal.*, 2010, **352**, 1805–1809.
13 C. Wang, Z. Tian, L. Wang, R. Xu, Q. Liu, W. Qu, H. Ma and B. Wang, *ChemSusChem*, 2012, **5**, 1974–1983.
14 M. Snåre, I. Kubičková, K. Eränen, P. Mäki-Arvela and D. Yu. Murzin, *Ind. Eng. Chem. Res.*, 2006, **45**, 5708–5715.
15 P. Mäki-Arvela, I. Kubičková, M. Snåre, K. Eränen and D. Yu. Murzin, *Energy Fuels*, 2007, **21**, 30–41.
16 B. Peng, Y. Yao, C. Zhao and J. A. Lercher, *Angew. Chem., Int. Ed.*, 2012, **51**, 2072–2075.
17 K. Murata, Y. Liu, M. Inaba and I. Takahara, *Energy Fuels*, 2010, **24**, 2404–2409.
18 R. W. Gosselink, D. R. Stellwagen and J. H. Bitter, *Angew. Chem., Int. Ed.*, 2013, **52**, 5089–5092.
19 S. A. W. Hollak, R. W. Gosselink, D. S. van Es and J. H. Bitter, *ACS Catal.*, 2013, **3**, 2837–2844.
20 J. Han, J. Duan, P. Chen, H. Lou, X. Zheng and H. Hong, *Green Chem.*, 2011, **13**, 2561–2568.
21 J. X. Han, J. Z. Duan, P. Chen, H. Lou and X. M. Zheng, *Adv. Synth. Catal.*, 2011, **353**, 2577–2583.
22 H. Yoshitake and Y. Iwasawa, *J. Catal.*, 1990, **125**, 227–242.
23 D. A. G. Aranda, A. L. D. Ramos, F. B. Passos and M. Schmal, *Catal. Today*, 1996, **28**, 119–125.
24 D. A. G. Aranda and M. Schmal, *J. Catal.*, 1997, **171**, 398–405.
25 S. J. Tauster, S. C. Fung and R. L. Garten, *J. Am. Chem. Soc.*, 1978, **100**, 170–171.
26 H. Yoshitake, K. Asakura and Y. Iwasawa, *J. Chem. Soc., Faraday Trans. 1*, 1989, **85**, 2021–2024.
27 A. Maeda, F. Yakamawa, K. Kunimori and T. Uchijima, *Catal. Lett.*, 1990, **4**, 107–112.
28 T. Uchijima, *Catal. Today*, 1996, **28**, 105–117.
29 A. Dandekar and M. A. Vannice, *J. Catal.*, 1999, **183**, 344–354.
30 W. Rachmady and M. A. Vannice, *J. Catal.*, 2002, **207**, 317–330.
31 P. Reyes, M. C. Aguirre, I. Melian-Cabrera, M. Lopez Granados and J. L. G. Fierro, *J. Catal.*, 2002, **208**, 229–237.
32 J. Sa, J. Bernardi and J. A. Anderson, *Catal. Lett.*, 2007, **114**, 91–95.
33 V. A. D. O'Shea, M. C. A. Galvan, A. E. P. Parts, J. M. Campos-Martin and J. L. G. Fierro, *Chem. Commun.*, 2011, **47**, 7131–7133.
34 S. Bonanni, K. Aït-Mansour, H. Brune and W. Harbich, *ACS Catal.*, 2011, **1**, 385–389.
35 T. Iizuka, Y. Tanaka and K. Tanabe, *J. Mol. Catal.*, 1982, **17**, 381–389.
36 M. A. Vannice, *Catal. Today*, 1992, **12**, 255–267.
37 A. Boffa, C. Lin, A. T. Bell and G. A. Somorjai, *J. Catal.*, 1994, **149**, 149–158.
38 A. T. Bell, *J. Mol. Catal. A: Chem.*, 1995, **100**, 1–11.
39 Y. Borodko and G. A. Somorjai, *Appl. Catal., A*, 1999, **186**, 355–362.
40 P. M. Maitlis and V. Zanottib, *Chem. Commun.*, 2009, 1619–1634.
41 Y. Nakagawa, M. Tamura and K. Tomishige, *ACS Catal.*, 2013, **3**, 2655–2668.
42 D. A. Ruddy, J. A. Schaidle, J. R. Ferrell III, J. Wang, L. Moens and J. E. Hensley, *Green Chem.*, 2014, **16**, 454–490.
43 S. Nishiyama, T. Hara, S. Tsuruya and M. Masai, *J. Phys. Chem. B*, 1999, **103**, 4431–4439.

